

Article

Spectral Relaxation Methodology for Chemical and Bioconvection Processes for Cross Nanofluid Flowing around an Oblique Cylinder with a Slanted Magnetic Field Effect

Ghulam Rasool ^{1,*}, Syed Zahir Hussain Shah ², Tanveer Sajid ³, Wasim Jamshed ³, Gilder Cieza Altamirano ⁴,
Bright Keswani ⁵, Rafaél Artidoro Sandoval Núñez ⁴ and Manuel Sánchez-Chero ⁶

¹ Institute of Intelligent Machinery, Faculty of Materials and Manufacturing, Beijing University of Technology, Beijing 100124, China

² Department of Statistics and Mathematics, Hazara University Mansehra, Mansehra 21300, Pakistan

³ Department of Mathematics, Capital University of Science and Technology, Islamabad 44000, Pakistan

⁴ Universidad Nacional Autónoma de Chota, Cajamarca, Perú-Fizmarko Research Group, Bogotá 110110, Colombia

⁵ Department of Computer Science & Engineering, Suresh Gyan Vihar University, Jaipur 302020, India

⁶ Facultad de Ingeniería de Industrias Alimentarias y Biotecnología, Universidad Nacional de Frontera, Sullana 20100, Peru

* Correspondence: grasool@zju.edu.cn



Citation: Rasool, G.; Shah, S.Z.H.; Sajid, T.; Jamshed, W.; Cieza Altamirano, G.; Keswani, B.; Artidoro Sandoval Núñez, R.; Sánchez-Chero, M. Spectral Relaxation Methodology for Chemical and Bioconvection Processes for Cross Nanofluid Flowing around an Oblique Cylinder with a Slanted Magnetic Field Effect. *Coatings* **2022**, *12*, 1560. <https://doi.org/10.3390/coatings12101560>

Academic Editors: George Kokkoris and Eduardo Guzmán

Received: 6 September 2022

Accepted: 12 October 2022

Published: 16 October 2022

Publisher's Note: MDPI stays neutral with regard to jurisdictional claims in published maps and institutional affiliations.



Copyright: © 2022 by the authors. Licensee MDPI, Basel, Switzerland. This article is an open access article distributed under the terms and conditions of the Creative Commons Attribution (CC BY) license (<https://creativecommons.org/licenses/by/4.0/>).

Abstract: The current investigation explains the chemical reaction and bioconvection process for an inclined magnetized Cross nanofluid over an inclined cylinder using a spectral relaxation approach. Additionally, the facts concerning swimming gyrotactic microorganisms, non-uniform thermal conductivity, and variable decrease or increase in heat sources are taken together. Each profile is checked for inclined and orthogonal magnetic impact. Appropriate transformations made for conversion of nonlinear PDEs into systems of ODEs. For obtaining numerical results, a spectral relaxation approach is utilized, and graphs are plotted with each physical parameter attached. It is well established that the temperature field intensifies owing to an amplification of thermal conduction and Brownian diffusivity phenomena. The heat transfer rate amplifies owing to a magnification in magnetic parameter and thermal conductivity, but the velocity field diminishes as a result of magnification in the Weissenberg number and power law index. Amplification in the reaction rate constant parameter diminishes the concentration field. Activation energy is the key factor responsible for magnification in the concentration field. Furthermore, smooth agreement is found during comparison with the existing literature. Statistical analysis is also conducted for physical quantities.

Keywords: spectral relaxation approach; Cross nanofluid; inclined cylinder; MHD; chemical reaction

1. Introduction

A generalized Newtonian fluid, whose viscosity is dependent on shear rate, is known as a Cross fluid. Because of its great effectiveness in industrial, chemical, and technological systems, generalized Newtonian fluids have recently attained great significance among researchers. Nabwey et al. [1] scrutinized the heat transfer in Carreau fluid poignant subjected to an inclined expanding cylinder. Their research also considers non-uniform thermal conductivity and an irregular decrease or rise in the heat source. The effects of the homogeneous-heterogeneous chemical reaction process (HHCP) and the Lorentz forces (LFs) on 3-D radiative magnetized the given Cross nanofluid were presented by Ayub et al. [2] utilizing two extending rotatory disks. Shah et al. [3] examined the thermal conductivity-based heat transfer in an MHD Cross nanofluid with Brownian motion, the notion of thermophoresis, and binary type of chemical reaction in the designated cylindrical coordinates. Ayub et al. [4] investigated the effects of changing thermal conductivity, Lorentz's force on an unstable Cross nanofluid, and the designated cylindrical coordinate.

Imran et al. [5] showed how non-linear heat radiation and melting events interact in a cross-nanofluid bioconvection flow with motile microorganisms. Hosseinzadeh et al. [6] demonstrated a cross-fluid flow with gyrotactic nanoparticles and microorganisms on a flat, three-dimensional geometrical cylinder with viscous dissipative force (dissipation) and a magnetic influence. Ali et al. [7] looked at the behavior of a cylinder that expands and contracts for a cross magnetized fluid flow with nanoparticles.

About 250 years have passed since the first mention of chemical reactions. Its roots were in ideas that described these processes as well as early experiments that categorized things as elements and compounds. The evolution of the idea of a chemically reactive fluid was important in forming chemistry as we distinguish it today. Chemical processes help our body grow and live. When we take medications, strike a match, or breathe, we experience reactions. The Casson nano liquid comprises bio convection phenomenon embedded with thermal radiation; magnetic dipole phenomenon flow subjected to an expandable cylinder was investigated in Khan et al. [8]. Gopal et al. [9] worked with a two-phase Carreau nanofluid flow with acceptable boundary conditions over a stretched cylindrical medium. Khan et al. [10] examined the effects of a stretching cylinder with a non-uniform heating source and sink, thermal radiation, Joule heating, together with homogeneous-heterogeneous chemical processes. The effects of chemical reaction, heat radiation, and the incoming porosity factor due to porous media on free stream convection and magnetized Carreau fluid flow toward a stretching cylindrical surface were examined in Lim et al. [11]. Liu et al. [12] looked at a stretching cylindrical surface with chemical reaction as well as the bio-convection and a radiative (nonlinear term appearing in it) Maxwell type nanofluid flow in a Darcy-Forchheimer (porous) medium. Alarabi et al. [13] demonstrated the hybrid nanofluid convection for Darcy medium with the involvement of heterogeneous-homogeneous chemical processes and magnetic impact characteristics past an extending or contracting cylindrical surface with the impact of Joule heating using $\text{Al}_2\text{O}_3 + \text{Cu}$ nanoparticles. Other recent studies related to chemical process with different facts such as activation energy and bi-convection Carreau nanofluid flow, stability of convection in a non-Newtonian vertical fluid, the Electroosmosis forces EOF-driven boundary layer flow, oxytactic microorganisms and nanoparticles, and the bio-thermal convection of Prandtl nanofluid have been made by [14–18].

Hannes Alfvén used the word “magnetohydrodynamics” for the first time in 1942, according to records. Its basis is in magneto, which is the magnetic field, hydro, which is water, and dynamics, which is motion. MHD is used in a diversity of technical and manufacturing applications, mostly in the nanotechnology sector. Due to the magnetic field’s numerous applications in the nuclear reactor, electrical furnace, installation of nuclear accelerators, turbo machinery, and blood flow, many researchers are excited to investigate its effects. Aly et al. [19] investigated how to incorporate magnetohydrodynamic (MHD) thermosolutal flow of a nanofluid in a squared dimensions of cavity with twofold rotation between an exterior circular cylindrical surface and an interior of cross-shaped. Zeeshan et al. [20] scrutinized the non-Newtonian Casson nanofluid’s magnetohydrodynamic transport caused by stretching a porous cylinder. Ramzan et al. [21] explained the magnetohydrodynamic (MHD) impact on well-known dusty Casson nanofluid over an overextended cylinder with inconstant heat source/sink and improved Fourier’s and Fick’s rules. In the presence of a chemically reactive species, Poply and Renu [22] examined the magnetohydrodynamic (MHD) impact on chemically reactive nanofluid flow across an extending cylinder with radiation effect. According to Ibrahim and Mekonnen [23], the combined convective heat flux rate of an MHD Williamson nanofluid across an elongating cylinder in the presence of a chemical reaction was affected by viscous dissipation and thermal radiation. A moving cylindrical surface with Brownian diffusion together with thermophoresis effects was investigated by Gharami et al. [24] for its uneven magnetohydrodynamic (MHD) free convection of tangent hyperbolic type nanofluid. Updated work on convection with Cross fluids is made by Xiong et al. [25]. Gowda et al. [26] investigated the influence of binary chemical reaction and activation energy on marangoni driven non-Newtonian fluid. Heat

and mass transfer effects on convection processes is elaborated as well [27–30]. Convective heat transport with attached Casson fluid is studied by Jyothi et al. [31]. The impact of exponential form of internal heat generation on water-based ternary hybrid nanofluid flow is disclosed by [32–39].

Bioconvection is the term used to describe the movement of many microscopic organisms in a fluid, particularly free-swimming zooplankton in water. Due to the flooding of these microorganisms, the bioconvection pattern is recognized as the creation of structures in microorganism suspensions, such as bacteria and algae. These microorganisms may be bacteria or algae. There is a torque reaction in gyrotactic bioconvection. Due to its uses in modelling oil and gas, gas-bearing sedimentary basins and bio-mechanics, bioconvection is widely employed. Ali et al. [40] investigated the preeminence of entropy generation (EG) in an MHD-bioconvective slip flow problem focusing Cross nanofluid comprehending gyrotactic microorganisms over an expanding cylinder. Yin et al. [41] investigated nonlinear phenomenon-based radiation on the bioconvection flow of magneto-Sisko fluid along an elongating cylinder. The magnetohydrodynamic boundary layer flow of a bioconvective Maxwell nanofluid over a horizontal cylinder that has been stretched exponentially was discussed in Ramzan et al. [42].

Abdel Malek et al. [43] demonstrated the effects of activation energy together with second-order slip on the bio-convection of Williamson-type nanofluid across an elongating cylinder with changing thermal conductivity. Magnetohydrodynamic natural convection of a CNT-water nanofluid incorporating a renovated Hamilton-Crosser model is utilized by Benos et al. [44]. The latest study regarding mixed convection with turbulent Hartmann flow and transitional regime is discussed by Sarris et al. [45,46], and Karvelas et al. [47] conducted micro scale heat transfer with convective conditions.

Novelty

- In the whole literature, there are several studies which are related to a Cross fluid model attached with horizontal and vertical cylinders, but a Cross fluid model has not yet been used with an inclined cylinder. Therefore, this attempt is performed to carry out the results with Cross fluid along an inclined cylinder geometry.
- The spectral relaxation technique has not been utilized yet for the case of numerical computation of Cross nanofluid flow subjected to an elastic cylinder.

2. Flow Analysis

Figure 1 portrays the performance of microorganisms; the magnetic phenomenon, in addition to the buoyancy phenomenon on a Cross liquid moving subjected to an inclined cylinder geometry, is shown by angle w , where the cylinder angle is Ω . The Buongiorno-based nanofluid model is considered in order to study the nanofluid impact on the Cross nanoliquid. The expanding rate of the cylinder is premeditated by $u_w = \frac{ax}{1-\xi t}$. The horizontal and normal direction for the case of fluid flow are 'x' and 'r' are Cartesian coordinates (u, v). The symbols g as well as γ^* indicate gravity and microorganisms' volume, respectively. The temperature is monitored in addition with sundry effects such as variation-based thermal conduction with no entrance of the nanoparticles at the cylinder surface. The insertion of microorganisms in Cross model fluid provide suspension to the nanofluid, and the activation energy phenomenon is considered. The Cross flow moves through electrical as well as magnetic paths, acting normal to the fluid flow pattern with a capacity for conducting electricity, which is denoted by the expression $B(t) = \frac{B_0}{(1-\xi t)^{\frac{1}{2}}}$, where the symbol B_0 is constant. The symbols T_w, C_w , and N_w indicate wall temperature as well as concentration and density phenomenon of the microorganisms. The free stream effect on temperature (T), concentration (C) field, and microorganisms (N) are T_∞, C_∞ , and N_∞ , respectively.

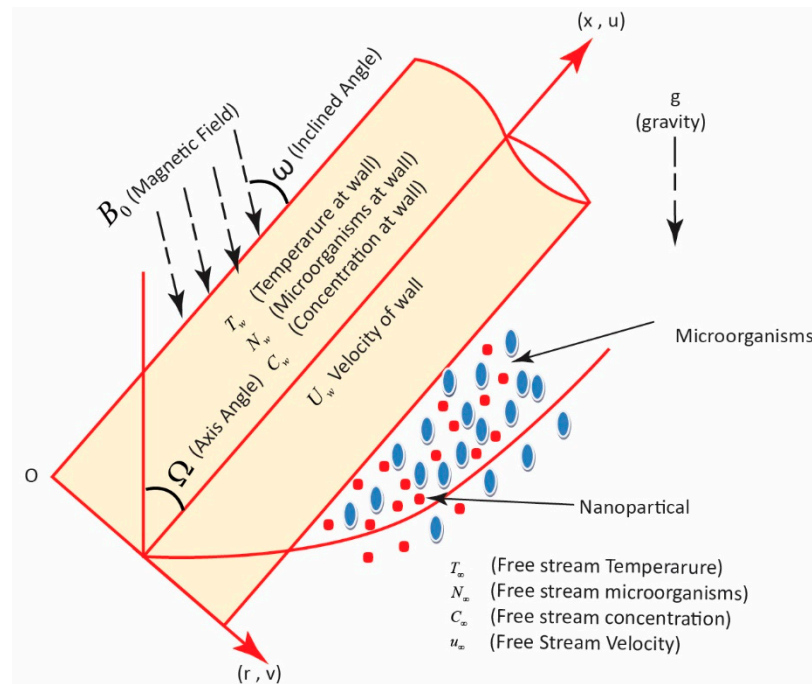


Figure 1. Physical configuration.

3. Rheology of Cross Fluid

The rheology of the Cross model is premeditated by

$$\frac{\mu - \mu_\infty}{\mu_0 - \mu_\infty} = \left(1 + (\dot{\gamma}\tilde{\gamma})^2\right)^{-1}$$

Herein, μ_∞ , μ_0 , and n signify the viscosities at unlimited and zero shear rates, and the material constant, together with the power-law index. The fluid behavior is Newtonian as a result of $n = 1$, and the thickness in shear for the case of $n < 1$ and $n > 1$ in the case of shear thinning. The free stream is denoted by $(\mu_\infty = 0)$. Therefore, $\mu = \mu_0 \left(1 + (\dot{\gamma}\tilde{\gamma})^2\right)^{-1}$. The expression regarding the rate at which fluid is working can be expressed as $\dot{\gamma} = \sqrt{\frac{1}{2}trA_1^2}$. The expression $A_1 = \nabla V + (\nabla V)^T$ indicates the tensor named after Rivlin–Erickson, whereas the expression V implies velocity. The expression of thermal based conductivity is [48]:

$$k_f = k_\infty \left(1 + \varepsilon \frac{T - T_\infty}{T_w - T_\infty}\right)$$

where ε and k_∞ stand for non-uniform as well as the ambient thermal conductivity.

4. Modeled Equations

In the light of above-mentioned effects and boundary layer assumptions, the equations regarding continuity, fluid flow momentum, temperature of the fluid flow, concentration phenomenon, and microorganism flow are enumerated underneath [49–51].

$$\frac{\partial}{\partial x}(ru) + \frac{\partial}{\partial r}(ru) = 0 \tag{1}$$

$$\begin{aligned} \frac{\partial u}{\partial t} + \left(u \frac{\partial}{\partial x} + v \frac{\partial}{\partial r}\right)u &= \mu_f \frac{1}{\left(1 + \tilde{\gamma}^n \left(\frac{\partial u}{\partial r}\right)^n\right)} - \frac{\sigma \sin^2(\omega) B_0^2}{\rho_f} u + \frac{g}{\rho_f} \left(\rho_f \beta_f (1 - C_\infty)(T - T_\infty)\right) \\ &+ (\rho_p - \rho_f)(C - C_\infty) - \gamma^* (\rho_m - \rho_f)(N - N_\infty) \cos \Omega - \mu_f \tilde{\gamma}^n \left(\frac{\partial u}{\partial r}\right)^n \frac{\partial^2 u}{\partial r^2} \left(1 + \tilde{\gamma}^n \left(\frac{\partial u}{\partial r}\right)^n\right)^{-2}, \end{aligned} \tag{2}$$

$$\frac{\partial T}{\partial t} + \left(u \frac{\partial}{\partial x} + v \frac{\partial}{\partial r}\right) u = \frac{1}{(\rho c_p)} \frac{1}{r} \left(\frac{\partial}{\partial r} \left(K_f \frac{\partial T}{\partial r}\right)\right) + j \left(D \frac{\partial T}{\partial r} \frac{\partial C}{\partial r} + \bar{D} \left(\frac{\partial T}{\partial r}\right)^2\right) \quad (3)$$

$$\frac{\partial C}{\partial t} + \left(u \frac{\partial}{\partial x} + v \frac{\partial}{\partial r}\right) C = \frac{D}{r} \frac{\partial}{\partial r} \left(r \frac{\partial C}{\partial r}\right) + \frac{\bar{D}}{T_\infty} \frac{1}{r} \left(r \frac{\partial T}{\partial r}\right) - K_r^2 (C - C_\infty) \left(\frac{\partial T}{\partial r}\right)^m e^{-\frac{E_0}{K^* T}} \quad (4)$$

$$\frac{\partial N}{\partial t} + \left(u \frac{\partial}{\partial x} + v \frac{\partial}{\partial r}\right) N = \frac{\bar{D}}{r} \frac{\partial}{\partial r} \left(r \frac{\partial N}{\partial r}\right) - \frac{b W_c}{r C_\infty} \frac{\partial}{\partial r} \left(r N \frac{\partial C}{\partial r}\right) \quad (5)$$

Symbols such as k_f , k_r , and W_c depict the thermal-based conductivity and reaction rate type constant, W_c depicts swimming capacity of the cells, and ρ_p indicates nanoparticle density. Abbreviations such as D , \bar{D} , and \bar{D} indicate diffusion phenomena in terms of Brownian, thermophoretics and microorganisms. Additionally, conditions at the boundary are premeditated by [52,53]

$$u = U_w, v = 0, T = T_w D \frac{\partial C}{\partial r} + \frac{\bar{D}}{T_\infty} \frac{\partial T}{\partial r} = 0, N = N_w \text{ at } r = R \quad (6)$$

$$u \rightarrow 0, T \rightarrow T_\infty, C \rightarrow C_\infty, N \rightarrow N_\infty, \text{ as } r \rightarrow \infty.$$

5. Method of Solution

Similarity variables to dimensionalize the above-mentioned equations are bestowed by [54]:

$$\eta = \frac{r^2 - R^2}{2R} \left(\frac{a}{v_f(1-\xi t)}\right)^{\frac{1}{2}}, \psi = \left(\frac{a v_f}{1-\xi t}\right)^{\frac{1}{3}} x R F(\eta) \quad (7)$$

$$\theta(\eta) = \frac{T - T_\infty}{T_w - T_\infty}, \phi(\eta) = \frac{C - C_\infty}{C_\infty}, \vartheta = \frac{N - N_\infty}{N_w - N_\infty}$$

Herein, $u = \frac{1}{r} \frac{\partial \psi}{\partial r}$ and $v = -\frac{1}{r} \frac{\partial \psi}{\partial x}$. A dimensionless system of equations is given by

$$\left(1 + \gamma(2 - n)\left(1 + We F''^2\right)^{-2}\right) \left(1 + n We F''^2\right) F'''' + (2 + (n - 1) We F''^2) + (2 + (n - 1) We F''^2) + FF'' - F'^2 - A \left(\frac{1}{2} \eta F'' + F'\right) - MF' + R_i(\theta - N_r \phi - R_b \vartheta) \cos \Omega = 0 \quad (8)$$

$$(1 + 2\gamma\eta) \left((1 + \theta\varepsilon)\theta'' + \theta'^2\varepsilon\right) + 2\gamma\theta'(1 + \varepsilon\theta) + Pr F\theta' - \frac{1}{2} A Pr \eta \theta' + Pr(1 + 2\gamma\eta)(Nb\theta'\phi' + Nt\theta'^2) = 0 \quad (9)$$

$$(1 + 2\gamma\eta)\phi'' + \left(2\gamma - \frac{1}{2} A L_e \eta\right)\phi' + L_e F\phi' + \frac{N_t}{N_b} (2\gamma\theta' + (1 + 2\gamma\eta)\theta'') - L_e K_r \phi(\delta\theta + 1)^m e^{-\frac{E}{\delta\theta + 1}} = 0 \quad (10)$$

$$(1 + 2\gamma\eta)\vartheta'' + \left(2\gamma - \frac{1}{2} A L_b \eta\right)\vartheta' + L_b F\vartheta' - P_e(\vartheta + w)(1 + 2\gamma\eta)(\phi'' + 2\gamma\phi') - P_e(1 + 2\gamma\eta)\phi\vartheta' = 0 \quad (11)$$

$$\left. \begin{aligned} F' = 1, & \quad F = 0, & \rho = 1, & \quad Nb\phi' + Nt\theta' = 0, & \vartheta = 1 & \quad \text{at } \eta = 0, \\ F' \rightarrow 0, & \quad \theta \rightarrow 0, & \phi \rightarrow 0, & \quad \vartheta \rightarrow 0 & \quad \text{when } \eta \rightarrow \infty. \end{aligned} \right\} \quad (12)$$

$We = \frac{a^3 x^2 r^2 \gamma^2}{(1-\xi t)^3 R^2 v_f}$ Weissenberg number, $\gamma = \left(\frac{(1-\xi t)v_f}{aR^2}\right)^{\frac{1}{2}}$ is the curvature parameter, $M = \frac{\sigma B_0^2}{a\rho_f}$ indicates the magnetic factor, $R_i = \frac{g\beta_f(1-C_\infty)(T_w-T_\infty)x}{u_w^2}$ is the mixed convection factor, $N_t = \frac{j(\bar{D}(T_w-T_\infty))}{v_f T_\infty}$ is the thermophoresis diffusion factor, $N_b = \frac{jDC_\infty}{v_f}$ is Brownian diffusion factor, $N_r = \frac{(\rho_p - \rho_f)C_\infty}{\beta_f \rho_f (1 - C_\infty)(T_w - T_\infty)}$ denotes the buoyancy force ratio factor, $Pr = \frac{\mu c_p}{k_f}$ is the Prandtl number, $Le = \frac{v_f}{D}$ is the Lewis number, $R_b = \frac{\gamma^*(\rho_p - \rho_f)}{\beta_f \rho_f (1 - C_\infty)(T_w - T_\infty)}$ is the bioconvection Rayleigh number, $L_b = \frac{v_f}{D}$ is the bioconvection Lewis number, $A = \frac{\xi}{a}$ is

the unsteadiness parameter, $P_e = \frac{v_f}{D}$ indicates the Peclet number, $K_r = \frac{K_r^2}{a}$ reflects the chemical reaction, $E = \frac{E_0}{K^*T_\infty}$ reflects the activation energy factor, $\delta = \frac{T_w - T_\infty}{T_\infty}$ indicates the difference in temperature, and $w = \frac{N_\infty}{N_w - N_\infty}$ reflects the change in microorganism concentration.

Physical quantities such as surface drag and heat transfer density for the case of microorganisms are mathematically designed and denoted as

$$C_f = \frac{\tau_w|_{r=R}}{\rho_f u_w^2}, Nu = \frac{xq_w|_{r=R}}{k_f(T_w - T_\infty)}, N_n = \frac{xq_n|_{r=R}}{D(N_w - N_\infty)} \tag{13}$$

Whereas symbols such as wall stress (τ_w), heat flux (q_w) and microorganism fluxes (q_n) are mathematically represented by the expressions enumerated below,

$$\tau_w = \mu_f \frac{\partial u}{\partial r} \left(1 + \tilde{\gamma} \left(\frac{\partial u}{\partial r} \right)^2 \right)^{\frac{n-1}{2}}, q_w = -k_f \left(\frac{\partial T}{\partial r} \right)_{r=R}, q_n = -\bar{D} \left(\frac{\partial N}{\partial r} \right)_{r=R} \tag{14}$$

Dimensionless C_f, Nu together with Nn are given by

$$Re^{1/2} C_f = F''(0) \left(1 + W_e F''(0)^2 \right)^{\frac{n-1}{2}}, Re^{-1/2} Nu = -\theta'(0), Re^{-1/2} N_n = -\vartheta'(0) \tag{15}$$

in which $Re = \frac{ax^2}{v_f(1-\xi t)}$ designates the Reynold number.

6. Numerical Procedure: Spectral Relaxation Technique

The spectral relaxation method (SRT), an original iterative technique, has been found to be particularly effective and practical for addressing nonlinear boundary value problems with semi-infinite interval definitions and some flow features that decay exponentially. The technique is obtained by importing the Gauss–Seidel concept of decoupling systems of equations and lines emerging from them by simply rearranging the order in which they are written and sequentially solved. A series of linear differential equations are formed by the algorithm’s controlling subsystems.

6.1. Advantages of Spectral Relaxation Technique

Spectral methods can be computationally:

1. Less expensive
2. Easier to implement than finite element methods
3. They shine best when high accuracy is sought
4. They are useful in simple domains with smooth solutions.

The flow chart of SRT is given in Figure 2.

6.2. Applied Spectral Relaxation Technique on Current Problem

Equations (9)–(12) and its related boundary conditions are solved using SRT. In this method, an SRM code is created using MATLAB software. The outlined steps for the SRM process are:

Step 1: the following iteration is obtained

$$F = F_{r+1}, \quad \theta = \theta_{r+1}, \quad \phi = \phi_{r+1}, \text{ and } \vartheta = \vartheta_{r+1} \tag{16}$$

Equations (9)–(11) take the form

$$\begin{aligned} & \left(1 + \gamma(2 - \eta) \left(1 + We F''_{r+1} \right)^{-2} \right) \left(1 + n We F''_{r+1} \right) F'''_{r+1} + (2 + (n - 1) We F''_{r+1}) + (2 + (n - 1) We F''_{r+1}) \\ & + F_{r+1} F''_{r+1} - F_{r+1}^2 - A \left(\frac{1}{2} \eta F''_{r+1} + F'_{r+1} \right) - MF'_{r+1} + R_i (\theta - N_r \phi_{r+1} - R_b \vartheta_{r+1}) \cos \Omega = 0 \end{aligned} \tag{17}$$

$$(1 + 2\gamma\eta) \left((1 + \theta_{r+1}\varepsilon)\theta''_{r+1} + \theta'^2_{r+1}\varepsilon \right) + 2\gamma\theta'_{r+1}(1 + \varepsilon\theta_{r+1}) + \text{Pr}F'\theta'_{r+1} - \frac{1}{2}A\text{Pr}\eta\theta'_{r+1} + \text{Pr}(1 + 2\gamma\eta)(Nb\theta'_{r+1}\phi'_{r+1} + Nt\theta'^2_{r+1}) = 0 \tag{18}$$

$$(1 + 2\gamma\eta)\phi''_{r+1} + \left(2\gamma - \frac{1}{2}AL_e\eta \right)\phi' + L_eF\phi'_{r+1} + \frac{N_t}{N_b}(2\gamma\theta'_{r+1} + (1 + 2\gamma\eta)\theta''_{r+1}) - L_eK_r\phi_{r+1}(\delta\theta_{r+1} + 1)^m e^{-\frac{E}{\delta\theta_{r+1}+1}} = 0 \tag{19}$$

$$(1 + 2\gamma\eta)\vartheta''_{r+1} + \left(2\gamma - \frac{1}{2}Al_b\eta \right)\vartheta' + L_bF\vartheta'_{r+1} - P_e(\vartheta_{r+1} + w)(1 + 2\gamma\eta)(\phi''_{r+1} + 2\gamma\phi'_{r+1}) - P_e(1 + 2\gamma\eta)\phi\vartheta'_{r+1} = 0 \tag{20}$$

$$\left. \begin{aligned} F'_{r+1} = 1, & \quad F_{r+1} = 0, & \quad \rho = 1, & \quad Nb\phi'_{r+1} + Nt\theta'_{r+1} = 0, & \quad \vartheta = 1 & \quad \text{at} & \quad \eta = 0, \\ F'_{r+1} \rightarrow 0, & \quad \theta_{r+1} \rightarrow 0, & \quad \phi_{r+1} \rightarrow 0, & \quad \vartheta_{r+1} \rightarrow 0 & \quad \text{when} & \quad \eta \rightarrow \infty. \end{aligned} \right\} \tag{21}$$

SPECTRAL RELAXATION TECHNIQUE

SRM is being utilized to solve the equation with associated boundary conditions equation 10. Linearizing the system of ODEs are taken place with Gauss–Seidel relaxation method. Current iterations are labeled by (r + 1) and previous are denoted by r. Step-wise SRM procedure is listed as

Step 1

$$f'_{r+1} = p_r, f_{r+1}(0) = 0$$

Step 2

In order to solve above system domain of transformation is made from to and here L is scaling parameter.

$$\begin{aligned} A_1 f_{r+1} &= T_1, & A_2 p_{r+1} &= T_2, & A_3 \theta_{r+1} &= T_3 \\ & & A_4 \phi_{r+1} &= T_4, & & \\ T_1 &= P_r, A_4 &= D^3, & & & \end{aligned}$$

Step 3

Diag () is diagonal matrix. is identity matrix and each of matrix has order (p + 1)x(p + 1) and p is grid points, Further process is

$$f_0 = s\eta + \frac{1-s}{1-\delta-\gamma}(1-e^{-\eta}), \quad p_0 = s + \frac{1-s}{1-\delta-\gamma}(e^{-\eta})$$

Figure 2. Flow chart of SRT.

Step 2: the following iteration is obtained

$$F'_{r+1} = S, F_{r+1}(0) = 0, \tag{22}$$

$$\begin{aligned} & \left(1 + \gamma(2 - \eta) \left(1 + WeS'^2_{r+1} \right)^{-2} \right) \left(1 + nWeS'^2_{r+1} \right) F'''_{r+1} + (2 + (n - 1)WeS'^2_{r+1}) + (2 + (n - 1)WeS'^2_{r+1}) \\ & + F_{r+1}S' - S^2_{r+1} - A \left(\frac{1}{2}\eta S' + S \right) - MS + R_i(\theta - N_r\phi_{r+1} - R_b\vartheta_{r+1}) \cos \Omega = 0, \end{aligned} \tag{23}$$

$$(1 + 2\gamma\eta) \left((1 + \theta_{r+1}\varepsilon)\theta''_{r+1} + \theta'^2_{r+1}\varepsilon \right) + 2\gamma\theta'_{r+1}(1 + \varepsilon\theta_{r+1}) + \text{Pr}S\theta'_{r+1} - \frac{1}{2}A\text{Pr}\eta\theta'_{r+1} + \text{Pr}(1 + 2\gamma\eta) \left(Nb\theta'_{r+1}\phi'_{r+1} + Nt\theta'^2_{r+1} \right) = 0, \tag{24}$$

$$(1 + 2\gamma\eta)\phi''_{r+1} + \left(2\gamma - \frac{1}{2}AL_e\eta \right) \phi' + L_eF\phi'_{r+1} + \frac{N_t}{N_b} (2\gamma\theta'_{r+1} + (1 + 2\gamma\eta)\theta''_{r+1}) - L_eK_r\phi_{r+1}(\delta\theta_{r+1} + 1)^m e^{-\frac{E}{\delta\theta_{r+1}+1}} = 0, \tag{25}$$

$$(1 + 2\gamma\eta)\theta''_{r+1} + \left(2\gamma - \frac{1}{2}Al_b\eta \right) \theta' + L_bF\theta'_{r+1} - P_e(\theta_{r+1} + w)(1 + 2\gamma\eta)(\phi''_{r+1} + 2\gamma\phi'_{r+1}) - P_e(1 + 2\gamma\eta)\phi\theta'_{r+1} = 0, \tag{26}$$

having boundary conditions

$$\left. \begin{aligned} F_{r+1} = 1, \quad F_{r+1} = 0, \quad \rho = 1, \quad Nb\phi'_{r+1} + Nt\theta'_{r+1} = 0, \quad \theta = 1 \quad \text{at} \quad \eta = 0, \\ F_{r+1} \rightarrow 0, \quad \theta_{r+1} \rightarrow 0, \quad \phi_{r+1} \rightarrow 0, \quad \theta_{r+1} \rightarrow 0 \quad \text{when} \quad \eta \rightarrow \infty. \end{aligned} \right\} \tag{27}$$

Step 3: the following is suitably solved as

$$f'_{r+1} = S, \quad f_{r+1}(0) = 0, \tag{28}$$

$$\left[\left(1 + \gamma(2 - \eta) \left(1 + WeS'^2_{r+1} \right)^{-2} \right) \left(1 + nWeS'^2_{r+1} \right) \right] S''_{r+1} + (2 + (n - 1)WeS'^2_{r+1}) - A\frac{1}{2}\eta S'_{r+1} + S_{r+1}[F_{r+1} - S_{r+1}] - S[A - M] + R_i(\theta - N_r\phi_{r+1} - R_b\theta_{r+1}) \cos \Omega = 0, \tag{29}$$

$$(1 + 2\gamma\eta)(1 + \theta_{r+1}\varepsilon)\theta''_{r+1} + \left[1 + 2\gamma(\eta\varepsilon + (1 + \varepsilon\theta_{r+1})) + \text{Pr}S - \frac{1}{2}A\text{Pr}\eta + \text{Pr}(1 + 2\gamma\eta)Nb\phi'_{r+1} \right] \theta'_{r+1} + \text{Pr}Nt\theta'^2_{r+1} = 0, \tag{30}$$

$$(1 + 2\gamma\eta)\phi''_{r+1} + \left(2\gamma - \frac{1}{2}AL_e\eta \right) \phi' + L_eF\phi'_{r+1} + \frac{N_t}{N_b} (2\gamma\theta'_{r+1} + (1 + 2\gamma\eta)\theta''_{r+1}) - L_eK_r\phi_{r+1}(\delta\theta_{r+1} + 1)^m e^{-\frac{E}{\delta\theta_{r+1}+1}} = 0, \tag{31}$$

$$(1 + 2\gamma\eta)\theta''_{r+1} + \left(2\gamma - \frac{1}{2}Al_b\eta \right) \theta' + L_bF\theta'_{r+1} - P_e(\theta_{r+1} + w)(1 + 2\gamma\eta)(\phi''_{r+1} + 2\gamma\phi'_{r+1}) - P_e(1 + 2\gamma\eta)\phi\theta'_{r+1} = 0. \tag{32}$$

Step 4: Scaling

Chebyshev pseudo-spectral association approach, where the range is changed from [0, L] to [-1, 1], proper alteration, and L is the parameter used for scaling purpose instead of η_∞ , is used to solve these decoupling equations.

$$\left. \begin{aligned} A_1S_{r+1} = B_1, \quad A_2\theta_{r+1} = B_2, \quad A_3\phi_{r+1} = B_3, \quad A_4\theta_{r+1} = B_4 \\ A = D^1, \quad B = Sr \\ A_2 = D^2 + \text{Diag}(\theta_{r+1})D \\ B_2 = \frac{1}{\left[(1 + \gamma(2 - \eta)(1 + WeS'^2_{r+1})^{-2})(1 + nWeS'^2_{r+1}) \right]} \left[\begin{aligned} (2 + (n - 1)WeS'^2_{r+1}) - A\frac{1}{2}\eta S'_{r+1} + S_{r+1}[F_{r+1} - S_{r+1}] \\ - S[A - M] + R_i(\theta - N_r\phi_{r+1} - R_b\theta_{r+1}) \cos \Omega \end{aligned} \right] \\ A_3 = \text{diag}((1 + \gamma(2 - \eta)(1 + We))(d + 1)) / d(D)^d D^2 + \text{diag}((1 + nWe))D + \text{diag}(\alpha)I \\ B_3 = \frac{1}{(1 + 2\gamma\eta)(1 + \theta_{r+1}\varepsilon)} \left[-1 - 2\gamma(\eta\varepsilon + (1 + \varepsilon\theta_{r+1})) + \text{Pr}S + \frac{1}{2}A\text{Pr}\eta - \text{Pr}(1 + 2\gamma\eta)Nb\phi'_{r+1} \right] \theta'_{r+1} - \text{Pr}Nt\theta'^2_{r+1} \\ A_4 = (1 + 2\gamma\eta)(1 + \theta_{r+1}\varepsilon)D^2 + \text{diag} \left(\left[-1 - 2\gamma(\eta\varepsilon + (1 + \varepsilon\theta_{r+1})) + \text{Pr}S + \frac{1}{2}A\text{Pr}\eta - \text{Pr}(1 + 2\gamma\eta)Nb\phi'_{r+1} \right] \right) D \\ B_4 = \left(2\gamma - \frac{1}{2}Al_b\eta \right) \theta' + L_bF\theta'_{r+1} - P_e(\theta_{r+1} + w)(1 + 2\gamma\eta)(\phi''_{r+1} + 2\gamma\phi'_{r+1}) - P_e(1 + 2\gamma\eta)\phi\theta'_{r+1} \end{aligned} \right\} \tag{33}$$

At this point, D as well as I indicate sloping and identity-type matrices; correspondingly, in the $(P + 1) \times (P + 1)$ order, P indicates points of grid structure. The SRT could be applied to a variety of physical and technical challenges in the future [55–58].

7. Validness of Study

In order to check the validation and authenticity of the obtained results, a comparison with Khan and Alshomrani [59] and Ragni et al. [60] has been undertaken in Table 1. From the obtained results, it is quite clear that the proposed scheme and obtained results are quite satisfactory and reliable. The domain of the scheme is considered $[0, L]$ to $[-1, 1]$. The mesh points are taken between $[-1, 1]$. From results mentioned below and displayed in the results and discussion, it is quite clear that the obtained results are quite satisfactory in the mesh points taken between $[-1, 1]$.

Table 1. A comparison of skin friction $-\text{Re}^{\frac{1}{2}}C_f$.

Γ	Khan and Alshomrani [59]	Ragni et al. [60]	Present
0.10	1.0000000	1.0000000	1.0000000
0.25	1.0943730	1.0943780	1.0943770
0.50	1.1887270	1.1887150	1.1887291
0.75	1.2818190	1.2818330	1.2818263
1.00	1.4533730	1.4593080	1.4533642

Figure 3 is designed to represent the comparison of the obtained outcomes with those reported by [59,60]. From comparison analysis it is quite evident that the obtained results are quite satisfactory and reliable.

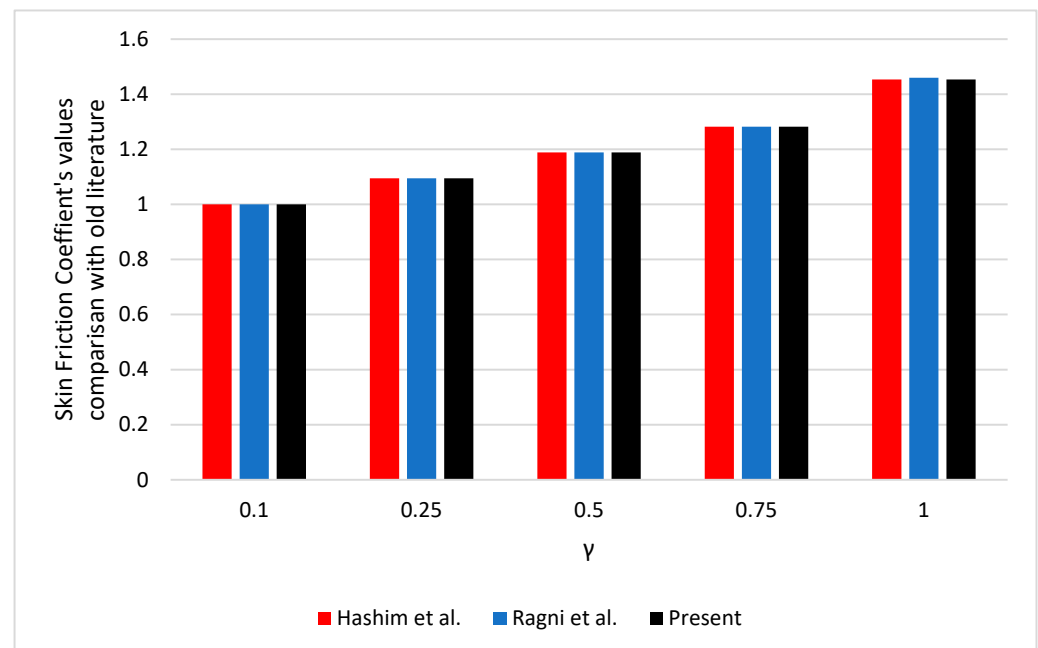


Figure 3. A comparison of skin friction in statistical form with [59,60].

8. Data Description, Collection, Interpretation, and Discussion

8.1. Data Collection

The modeled system of PDEs are derived using the law of conservation of momentum, Newton's second law of motion, second law of thermodynamics, and Fick's second law of diffusion. Boundary layer approximation has been applied to intricate effects such as viscous dissipation.

8.2. Data Description

Equation (1) describes the continuity equation. The movement of fluid flow is described by Equation (2), which is derived under the light of Newton's second law of motion. Effects such as bio convection, MHD, and inclined magnetic field are considered in order to study the shear thinning/thickening nature of the fluid in terms of model flexibility. The temperature aspect of the fluid is mentioned in Equation (3). Thermal conductivity and the Buongiorno nanofluid model are taken to investigate the temperature phenomenon of the fluid. Mass transport inside the fluid is mentioned by Equation (4) with the inclusion of effects such as nanofluids and activation energy. Microorganisms moving through a nanofluid is mentioned by Equation (5). Suspension of nanoparticles in the fluid is greatly strengthened in the presence of microorganisms.

8.3. Data Handling

After the application of the similarity variable, the modeled PDEs renovated into ODEs are handled numerically with the utilization of the well-established spectral relaxation method. The detailed procedure of spectral relaxation method is mentioned in the numerical procedure section.

8.4. Interpretation of Numerically Outcomes

The behavior of the dimensionless parameters appearing during numerical simulation of the problem are scrutinized in the light of drag friction, the heat deliverance phenomenon and microorganisms' density. Novel effects such as an inclined magnetic field in terms of inclined Cross fluid is considered. It is well established that an amplification in We amplifies temperature and diminishes the phenomenon. The velocity of fluid diminishes owing to an incremental change in inclined MHD angle ω . The detail of obtained outcomes are presented in the Results and Discussion section.

9. Results and Discussion

This section is structured to investigate the sundry parameters' effect on velocity, temperature, concentration, heat, and mass flux; density of motile microorganisms' profiles are discussed in the form of figures and tables as well. Table 2 displayed the Weissenberg number (We), bioconvection Rayleigh number (Rb), power law index (n), curvature parameter (γ), magnetic parameter M , unsteadiness parameter (A) against surface friction, heat deliver rate, and microorganisms' density. Through amplification in We , Rb escalates C_f but diminishes for parameters such as n , γ , M , and A . The rate at which heat is delivered amplifies for all distinguished parameters, and the microorganisms' density phenomenon diminishes for We , Rb , n , γ , and M and amplifies in the case of A . It is observed that that the surface drags and heat deliverance rate amplifies as a result of an amplification in We . Relaxation of the fluid escalates by the virtue of a magnification in We , which decreases and amplifies the drag phenomenon and heat deliverance rate but decreases microorganisms' density. It is well established that a positive variation in bio convective Rayleigh number Rb amplifies buoyancy forces, and this change produces a decrement in the velocity field, which amplifies drag phenomenon. Microorganism's density diminishes in the case of $0 \leq Rb \leq 1$ and increases in the case of $1 \leq Rb \leq \infty$. The heat deliverance rate amplifies owing a positive variation in Rb . It is noticed that the fluid behavior is shear thickening in the case of $n > 1$, and shear thinning for $n < 1$. Viscous forces dominate the inertial forces, which lessens the fluid motion, density of microorganisms, and increases the fluid temperature. It is quite clear that the fluid is allowed to relax and regain its original shape, similar to an elastic rubber that magnifies the fluid viscosity. An amplification in Γ provides a resistance to the fluid flow and, moreover, produces a decrement in drag phenomenon and microorganisms' density but amplifies temperature at the other end. The Lorentz force is produced as a result of a positive variation in M , which acts like a barrier in the way of fluid flow which reduces drag phenomenon, microorganism's density, and increases temperature. It is observed that fluid behavior is unsteady as a result of an

incremental change in A because the viscosity of fluid increases, which lessens the surface drag phenomenon, microorganism’s density, and amplifies the heat deliverance rate.

Table 2. Influence of various sundry parameters on surface drag frictiuon, heat transfer as microorganism’s density.

We	R _b	N	Γ	M	A	Surface Drag Friction Cf	Heat Transfer Nu	Microorganisms’ Density Nn
1.0	-	-	-	-	-	1.235892	1.02357	0.985636
10.0	-	-	-	-	-	1.259863	1.033987	0.965874
25.0	-	-	-	-	-	1.278524	1.042548	0.947865
50.0	-	-	-	-	-	1.298552	1.053952	0.925479
-	0.10	-	-	-	-	1.309874	1.07899	0.995687
-	0.15	-	-	-	-	1.324587	1.098745	0.987541
-	0.25	-	-	-	-	1.345469	1.102155	0.978745
-	0.35	-	-	-	-	1.369874	1.112548	0.964587
-	-	0.50	-	-	-	1.121548	1.087855	1.124579
-	-	0.80	-	-	-	1.102545	1.103215	1.112459
-	-	1.10	-	-	-	1.087854	1.125449	1.101255
-	-	1.35	-	-	-	1.069874	1.145687	1.096548
-	-	-	1.0	-	-	1.045698	1.101255	1.095785
-	-	-	2.0	-	-	1.032578	1.111854	1.092549
-	-	-	3.0	-	-	1.026548	1.125487	1.091458
-	-	-	4.0	-	-	1.01236	1.135459	1.089652
-	-	-	-	0.10	-	1.894521	1.884579	1.884578
-	-	-	-	0.50	-	1.890023	1.889578	1.874578
-	-	-	-	1.00	-	1.880457	1.890022	1.86458
-	-	-	-	1.12	-	1.874587	1.898453	1.846578
-	-	-	-	-	0.10	1.564874	1.601254	1.615458
-	-	-	-	-	0.15	1.554248	1.614588	1.624578
-	-	-	-	-	0.25	1.542154	1.624574	1.634588
-	-	-	-	-	0.35	1.532645	1.631246	1.641249

9.1. Velocity Profile

Figures 4 and 5 are premeditated to study the effect of the Weissenberg number *We* and inclined angle ‘*w*’ on the velocity field $f'(\eta)$. The Weissenberg number is the relaxation time required by the fluid to relax to recuperate its original shape. Shear coagulating behavior is described in the case of a magnification in ‘*We*’. Boundary layer thickness decreases, and fluid moves towards the wall owing to a magnification in *We* from 0.3 to 1.4. Velocity decreases owing to a magnification in the inclined angle from 0 to $\frac{\pi}{2}$, which lessens $f'(\eta)$. It is well established that the velocity field $f'(\eta)$ diminishes by virtue of an amplification in inclined angle *w*. As the angle amplifies, the parallel component diminishes, and the vertical component escalates. It is discovered that there is an inverse relationship between *w* and fluid velocity, meaning the velocity field decreases owing to a magnification in *w*. An increase in *w* around the x-axis significantly increases the gravity component due to $\cos\Omega$, which reduces the buoyancy force and weakens the driving force, causing the flow rate to decrease while velocity decreases. Figures 6 and 7 displayed the influence *n* and *M* on $f'(\eta)$. The parameter *n* is the fluid parameter that determines how viscous the fluid is. The fluid thins in terms of shear ($n < 1$), thickening ($n > 1$), and Newtonian ($n = 1$). The shear thickening trend is reported in the case of a magnification in *n*. Paint is an example of this phenomenon. It is observed from the figure that the boundary layer thickness (BLT) diminishes, and the fluid approaches the vertical wall by virtue of an enhancement in *n* from 0.1 to 1.6. It is quite clear from the figure that the velocity factor diminishes more rapidly for the vertical angle in contrast to the inclined angle *w*. The fluid moving through the electric as well as the magnetic field produces the Lorentz force. The force acts like a barrier in the way of fluid flow. The Lorentz force is inversely related to the velocity. The velocity diminishes owing to a magnification in *M*. This decrement in velocity is more

dominant in the case of no inclined angle in comparison to the inclined angle ' w '. That is why an amplification in M ranges from 0 to 3 strengthens the Lorentz force phenomenon and decreases $f'(\eta)$, as shown in Figure 7. The effect of curvature parameter ' γ ' is shown in Figure 8. It concludes that by growing the said parameter, the velocity of fluid decreases, when actually, the curvature is the bending rate of fluid particles, and because of this, linear velocity decreases.

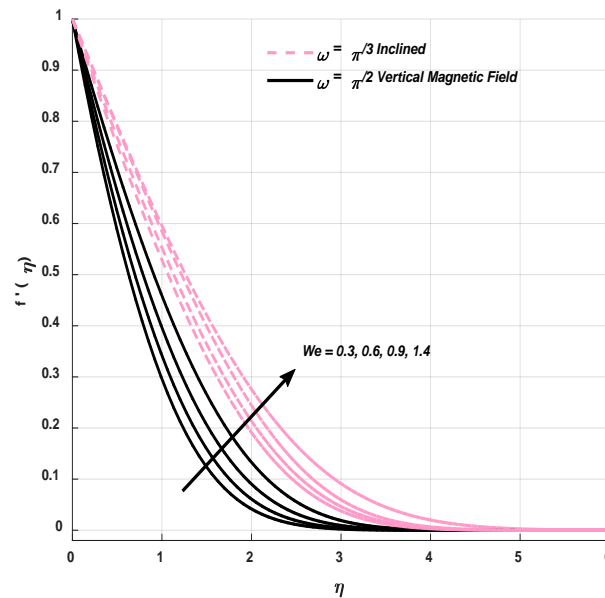


Figure 4. Revealing the performance of We against $f'(\eta)$.

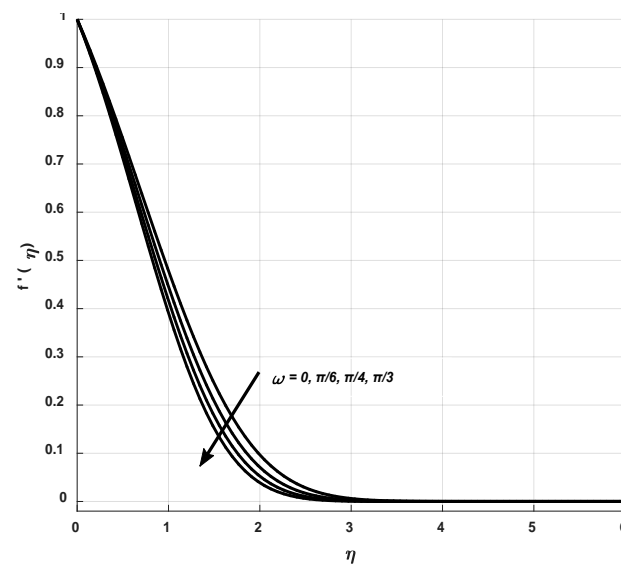


Figure 5. Exposure of w against $f'(\eta)$.

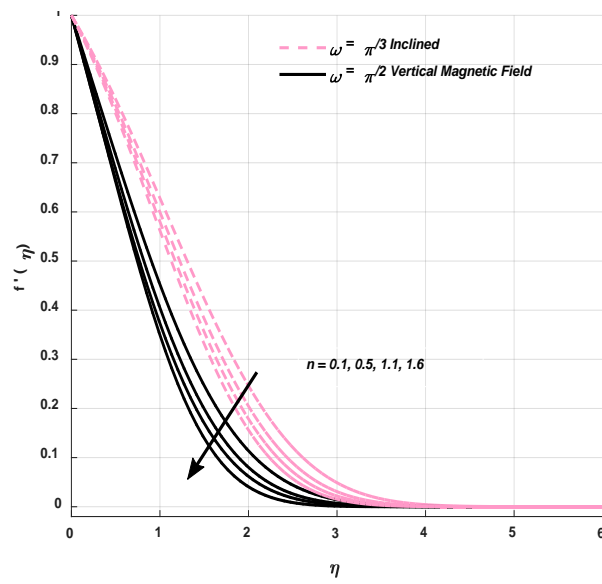


Figure 6. Disclose the effect of n versus $f'(\eta)$.

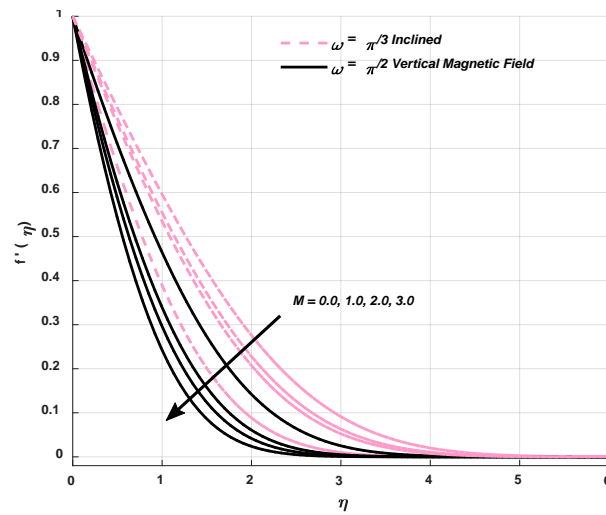


Figure 7. Reveal the impact of M against $f'(\eta)$.

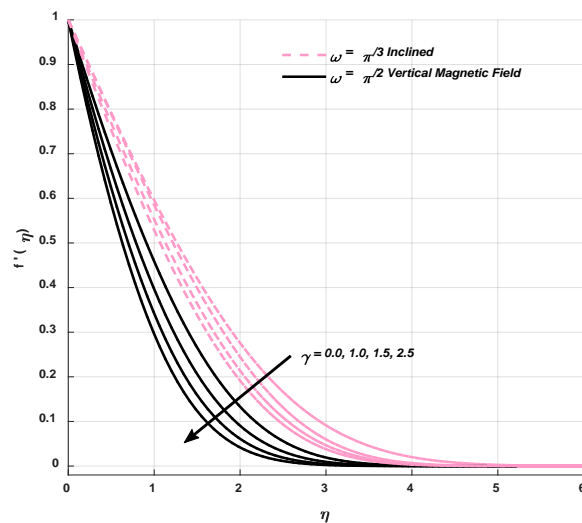


Figure 8. Reveal the impact of γ against $f'(\eta)$.

9.2. Temperature Profile

The impact of Weissenberg number We and thermal conductivity ϵ on the temperature field $\theta(\eta)$ are displayed in Figures 9 and 10. It is observed from Figure 4 that an amplification in We amplifies the fluid viscosity. In the light of Figure 3, a positive variation in viscosity amplifies the fluid temperature. The thermal boundary layer thickness (TBL) is amplified, and fluid moves away from the wall in an upward direction, owing to a magnification in the We ranges from 1 to 4. As a result, the temperature field escalates as shown in Figure 9. The Weissenberg number relies on the relaxation time, or the time required by the fluid to relax and regain its original position. Fluid becomes more viscous as a result of magnification in We . Shear thickening behavior is observed in the case of a magnification in We , which escalates the temperature phenomenon. The ability of any material to conduct heat is called thermal conductivity. In liquids, the thermal conductivity phenomenon takes place as a result of an intermolecular collision, which furthermore amplifies the temperature of the amplified fluid. Molecules collide more frequently as a result of a magnification in ϵ and share more K.E with each other, and the heat transfer exchange phenomenon of this situation intensifies more favorably in the case of nanofluids. The fluid flows away from the wall and TBL escalates in the case of a positive variation in ϵ from 1 to 5.5, as displayed in Figure 10. Figures 11 and 12 highlighted the influence of Prandtl number Pr and inclined angle ω on $\theta(\eta)$. The Prandtl number is the ratio of momentum to thermal diffusivity. Heat diffuses more by the virtue of an increment in Pr , which lessens the temperature inside the fluid. The fluid approaches towards the vertical wall and TBL abates. The abatement in $\theta(\eta)$ is more dominant in the case of no inclined angle, in comparison to inclined angle ω , as displayed in Figure 11. From Figure 12 it is observed that a magnification in ω amplifies $\theta(\eta)$. The viscosity of fluid diminishes as a result of an augmentation in ω , which furthermore lessens the velocity and ultimately escalates the temperature phenomenon. That is why an amplification in ω is the major factor responsible for an increment in TBL. The impact of curvature parameter γ is shown in Figure 13. Enhancing the curvature parameter bending of fluid particles increases the resistance within the wall, causing the rise in temperature.

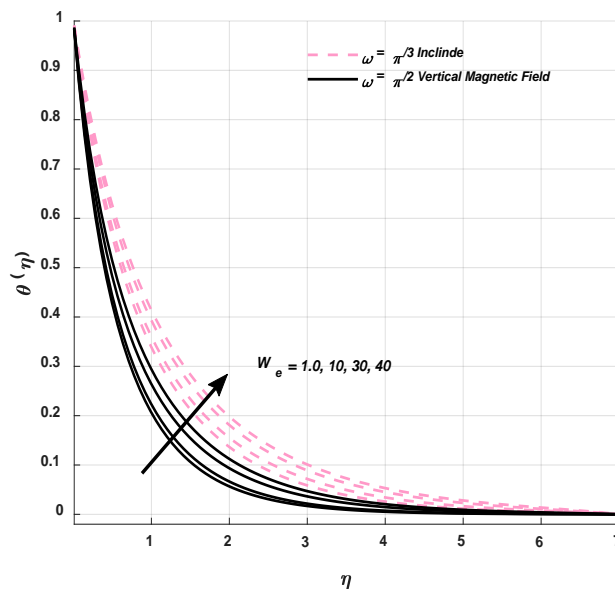


Figure 9. Influence of We on temperature field $\theta(\eta)$.

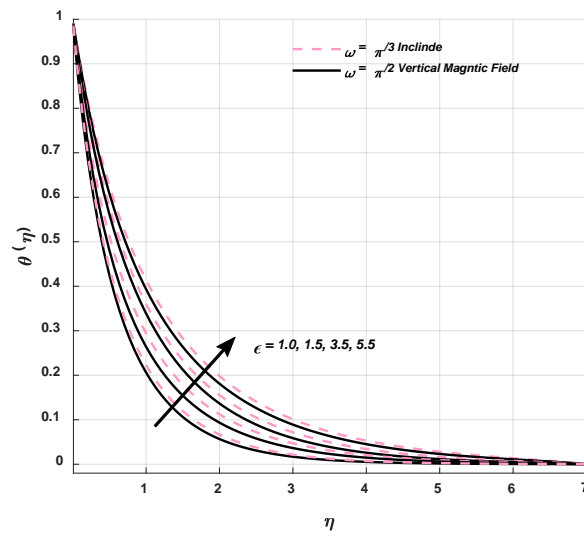


Figure 10. Impact of ϵ on $\theta(\eta)$.

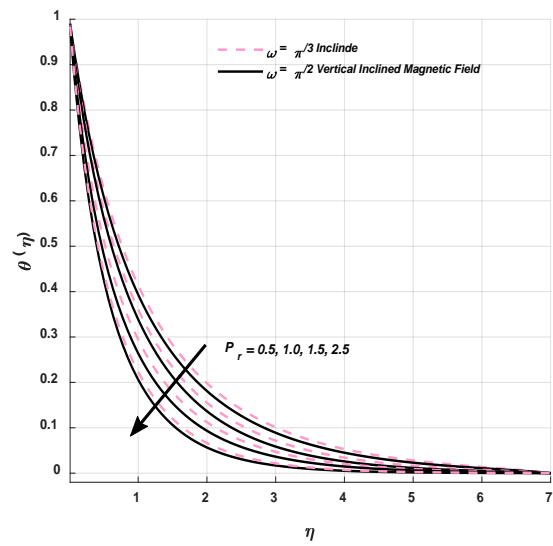


Figure 11. Effect of Pr on $\theta(\eta)$.

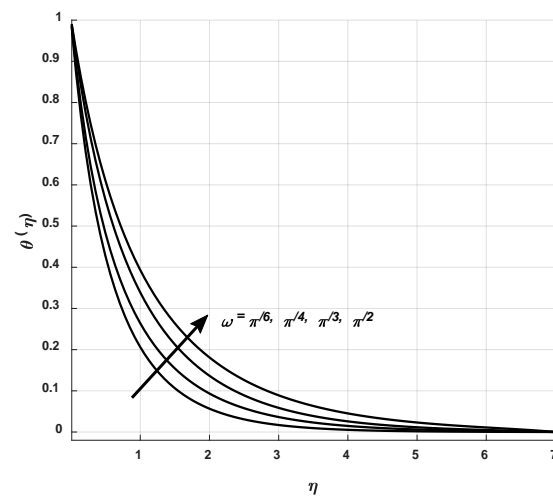


Figure 12. Behavior of ω on $\theta(\eta)$.

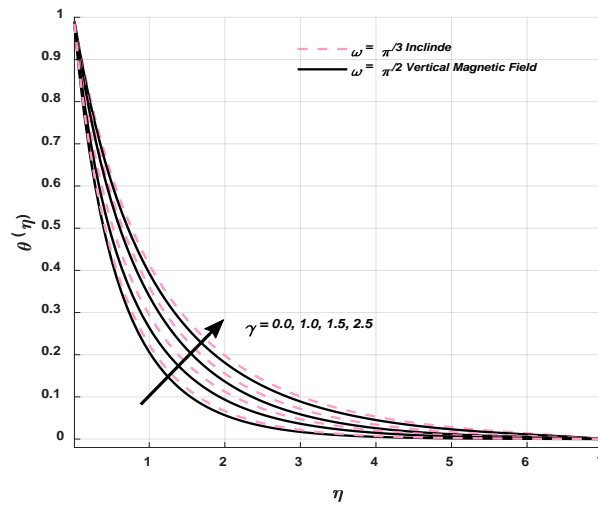


Figure 13. Behavior of γ on $\theta(\eta)$.

9.3. Concentration Profile

Figures 14 and 15 highlighted the influence of We and reaction rate constant K_r on the concentration field $\phi(\eta)$. It is observed that a positive change in We diminishes the concentration phenomenon. The concentration boundary layer thickness decreases and moves forward, owing to the magnification of We , as shown in Figure 14. Reaction rate K_r is directly proportional to concentration. Concentration of the fluid diminishes owing to a variation in K_r , which depreciates the concentration boundary layer thickness as fluid moves towards the wall in a downward direction, as shown in Figure 15. The effect of thermal conductivity ε on the mass fraction field is highlighted in Figure 16. The temperature amplifies owing to a magnification in ε , which diminishes the viscosity phenomenon and concentration of the fluid as well. The velocity of fluid decreases owing to a magnification in ω . Velocity is linked with the viscosity phenomenon. A positive variation in ω diminishes the viscosity and concentration field $\phi(\eta)$ as shown in Figure 17.

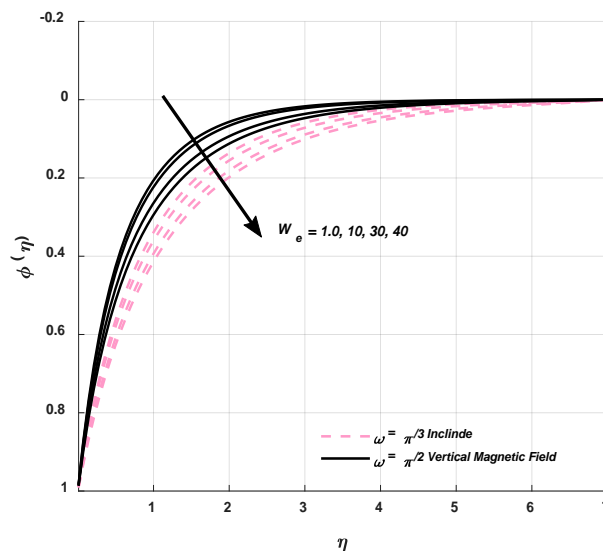


Figure 14. Effect of We on mass fraction field $\phi(\eta)$.

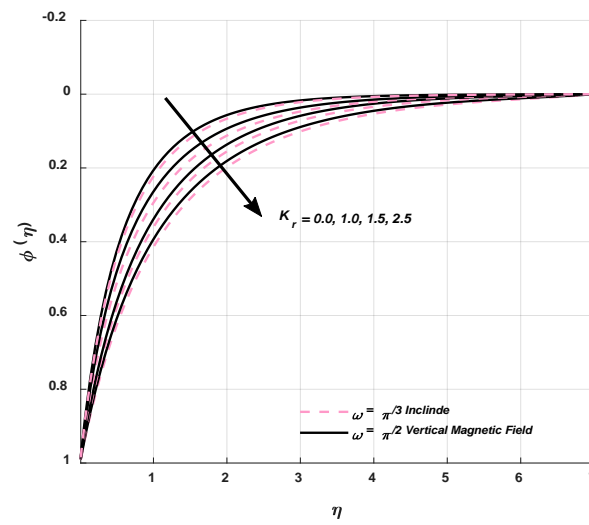


Figure 15. Impact of K_r on $\phi(\eta)$.

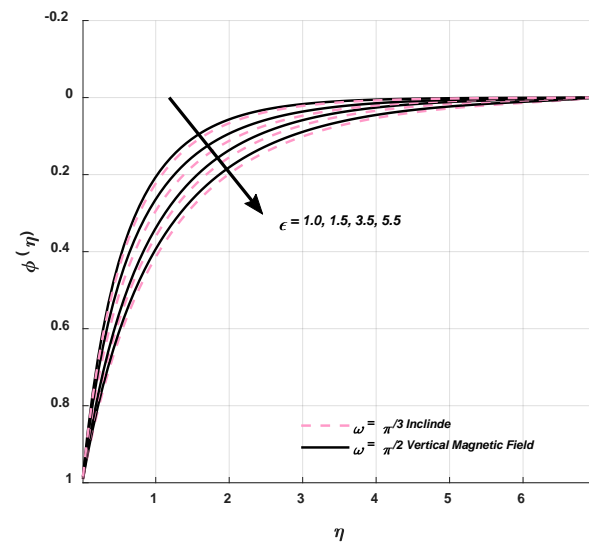


Figure 16. Influence of ϵ on $\phi(\eta)$.

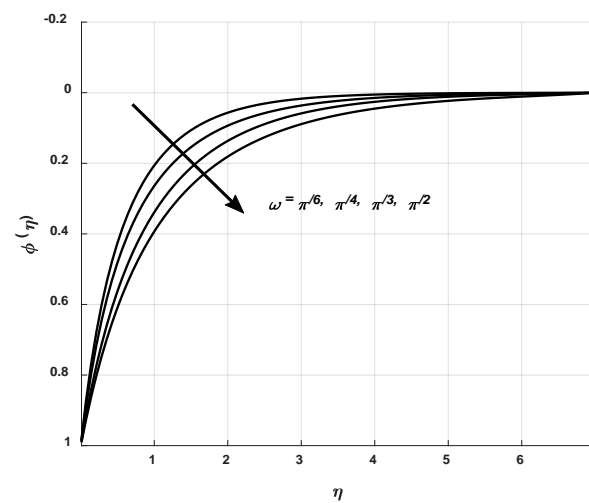


Figure 17. Influence of w on $\phi(\eta)$.

9.4. Statistical Graphs

Figures 18–20 are designed to reflect the impact of We , Rb , and n on the drag coefficient, heat transfer, and motile density of microorganisms. Weissenberg is directly linked with relaxation time. Surface drag is inversely related to fluid viscosity. It is observed that a variation in relaxation time increases fluid viscosity, which diminishes the fluid velocity and amplifies skin friction coefficient. Viscosity is inversely linked with temperature. Physical aspects such as Nu_x and Nn_x diminish, owing to an amplification in viscosity. Amplification in Rb escalates surface drag phenomenon much better in contrast to heat transfer and motile density of microorganisms, as displayed in Figure 19. Figure 20 displayed the effect of power law index n on various physical quantities. The power law index is related to the viscosity phenomenon and is opposite to the temperature effect, and shear thickening behavior is reported by the virtue of a magnification in n , which amplifies the surface drag and density of motile microorganisms and diminishes the heat transfer phenomenon. Fluid behavior is shear thinning for $n < 1$, Newtonian for $n = 1$, and ashear thickening in the case of $n > 1$. Blood is a perfect example of this phenomenon. Blood behavior is shear thinning and shear thickening according to the situation. That is why magnification diminishes velocity and magnifies temperature. Figures 21–23 are designed to highlight the influence of γ , M , and A on various physical quantities. It is observed that an enhancement in γ amplifies the fluid velocity and lessens the drag phenomenon of the surface and microorganism's density but magnifies the heat transfer rate. It is well established that an amplification in curvature parameter amplifies the fluid viscosity phenomenon, which diminishes the velocity of fluid flow and amplifies temperature because viscosity is inversely linked with temperature. Paint is the example of this phenomenon. Fluid possessing electric current when moving through a magnetic creates a resistive-type force, known as the Lorentz force. The Lorentz force is basically a resistive force that diminishes the drag surface phenomenon and density of motile microorganisms. This resistive force, on the other hand, amplifies the fluid temperature and heat transfer rate of the fluid depicted in Figure 22. The influence of unsteady parameter A on the surface drag coefficient, heat transfer, and motile microorganisms are highlighted in Figure 23. It is quite evident that an augmentation in an unsteady phenomenon brings about a magnification in fluid viscosity. This augmentation in viscosity is a major factor responsible for a decrement in fluid velocity. Velocity of fluid is inversely related to drag phenomenon of a surface. That is why an amplification in A diminishes the surface drag friction. Density is also related to viscosity. The fluid is denser when the viscosity amplifies, which is why an abatement in fluid viscosity lessens the density of motile microorganisms.

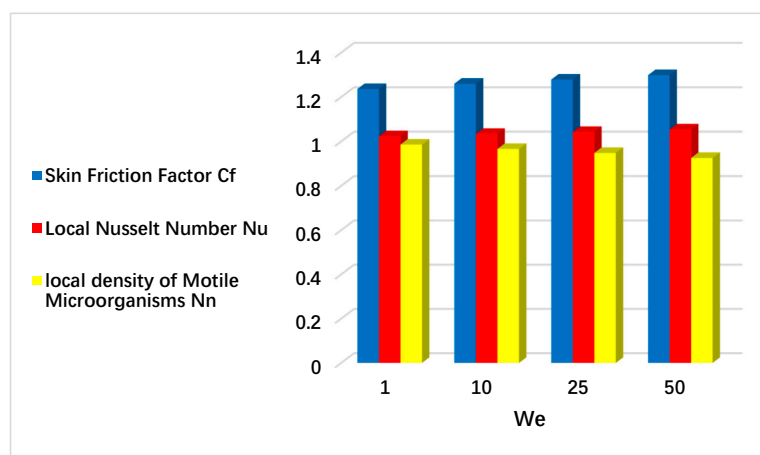


Figure 18. Influence of We against C_f , Nu , and Nn .

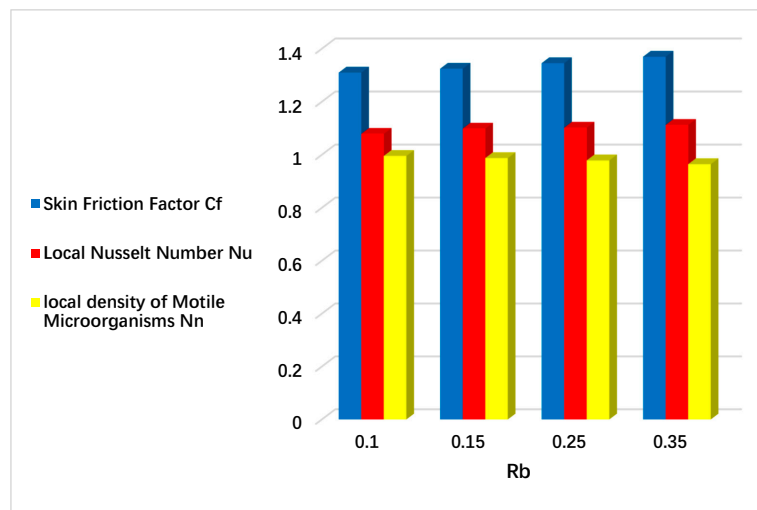


Figure 19. Influence of Rb on C_f , Nu , and Nn .

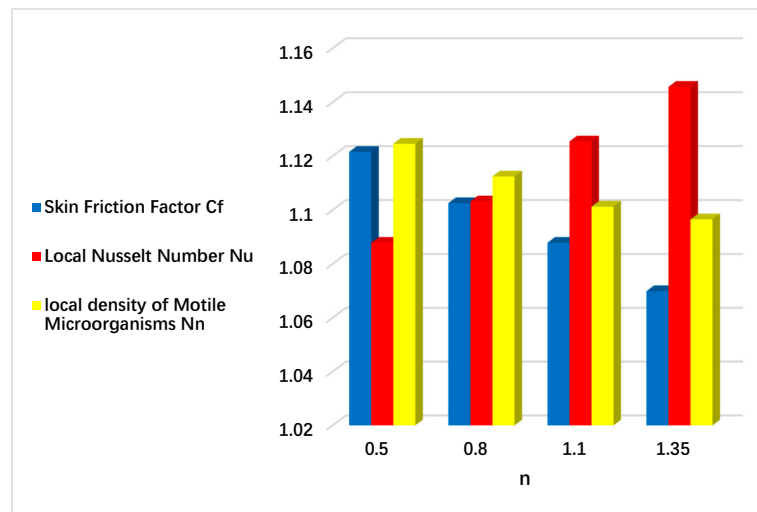


Figure 20. Impact of n on C_f , Nu , and Nn .

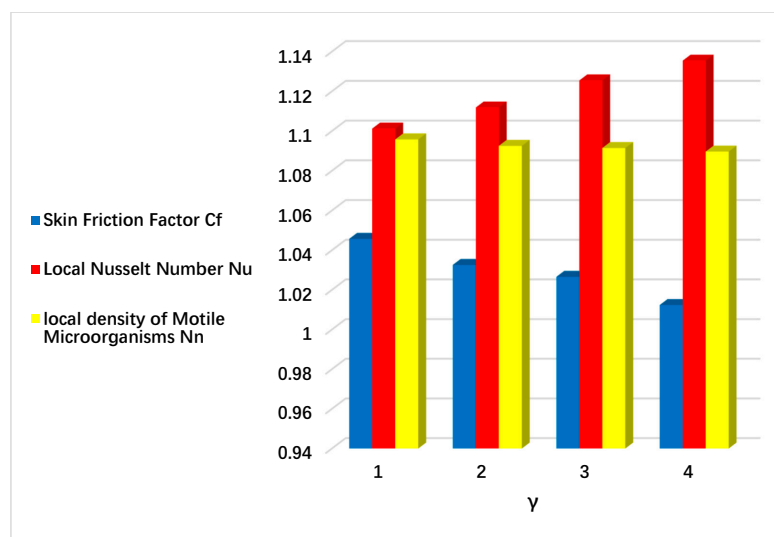


Figure 21. Effect of γ on C_f , Nu , and Nn .

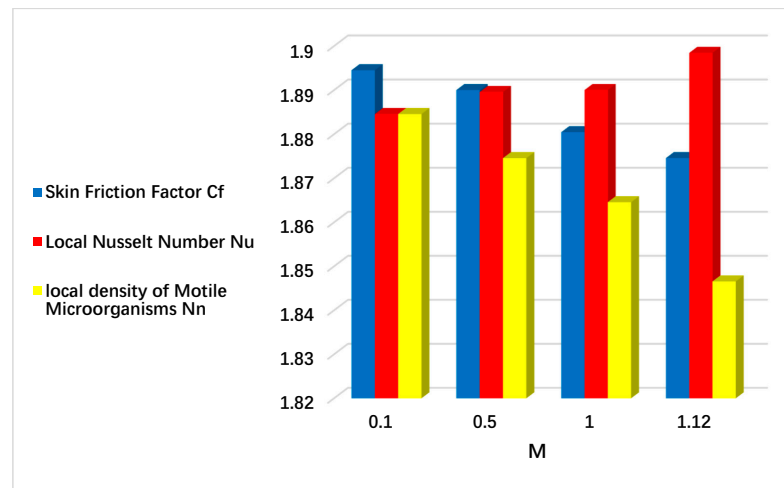


Figure 22. Influence of M on C_f , Nu , and Nn .

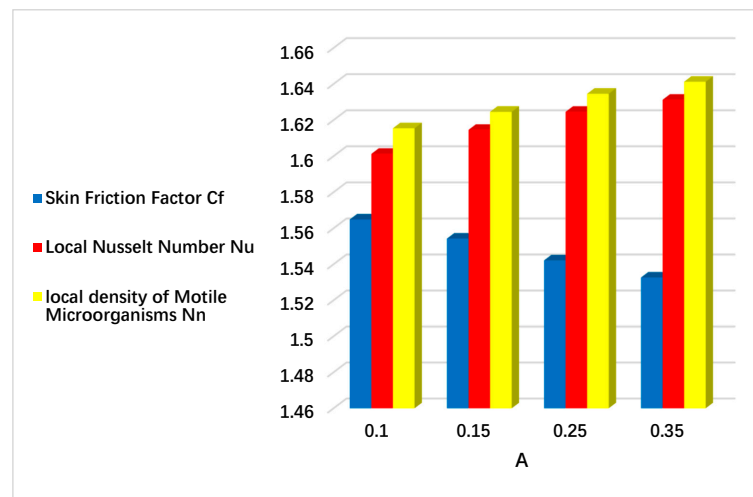


Figure 23. Impact of A on C_f , Nu , and Nn .

10. Conclusions

In this article, there is scrutiny regarding the chemical reaction and bioconvection process for an inclined magnetized Cross nanofluid over an inclined cylinder using the spectral relaxation approach. Regarding swimming gyrotactic microorganisms, non-uniform thermal conductivity and variables decreasing or increasing in heat source are taken together. The key points are listed below:

- i. Shear thinning behavior is noticed as a result of a magnification in a Weissenberg number, which brings a decrement in fluid viscosity and amplifies velocity of the fluid flow.
- ii. The fluid behavior is shear thickening owing to magnification in power law index n , which amplifies the fluid viscosity and velocity phenomenon.
- iii. It is well-established that the molecules collide more randomly and exchange more KE with each other by virtue of a magnification in the thermal conductivity parameter ε , which provides an amplification in the temperature field.
- iv. It is observed that the microorganism swimming speed amplifies as a result of an augmentation in w , which brings about an increment in the microorganisms flow field.

- v. Transport of heat is rapid on a cylinder as compared to a flat surface. Molecules collide more randomly and enhance K.E in the case of cylindrical surface in contrast to elastic surface.
- vi. The drag friction phenomenon is inversely related to the fluid flow motion. Amplification in We amplifies and encourages the viscosity phenomenon, which diminishes the fluid velocity and escalates the drag friction phenomenon.
- vii. Viscosity is inversely linked with temperature. Amplification in Weissenberg number We and power law index n amplifies the fluid viscosity, which diminishes the fluid velocity and amplifies temperature.
- viii. A positive variation in M encourages the resistive force, called Lorentz force, which provides hurdle to the fluid flow and diminishes the velocity phenomenon, but a magnification M provides a substantial heat to the fluid flow subjected to a cylinder.
- ix. From the obtained results, it is revealed that more heat is produced in the case of nanofluid in contrast to simple base fluid.

Author Contributions: Conceptualization, G.R., S.Z.H.S., T.S., W.J., G.C.A., B.K., R.A.S.N., and M.S.-C.; Data curation, T.S.; Formal analysis, G.R., S.Z.H.S., W.J., G.C.A., B.K., R.A.S.N., and M.S.-C.; Funding acquisition, G.R.; Investigation, G.R., T.S., and W.J.; Methodology, S.Z.H.S., W.J., and R.A.S.N.; Project administration, G.R.; Resources, G.C.A. and R.A.S.N.; Software, G.R., S.Z.H.S., and W.J.; Supervision, M.S.-C.; Validation, T.S.; Visualization, G.R., S.Z.H.S., G.C.A., and B.K.; Writing—original draft, G.R., S.Z.H.S., T.S., W.J., G.C.A., B.K., R.A.S.N., and M.S.-C.; Writing—review and editing, G.R., S.Z.H.S., T.S., W.J., G.C.A., B.K., R.A.S.N., and M.S.-C. All authors have read and agreed to the published version of the manuscript.

Funding: This research received no external funding.

Institutional Review Board Statement: Not Applicable.

Informed Consent Statement: Not Applicable.

Data Availability Statement: The numerical data used to support the findings of this study are included within the article.

Conflicts of Interest: The authors declare no conflict of interest.

Nomenclature

Parameters	Units	Parameters	Units
Gravity (g)	$\frac{m}{s^2}$	Activation energy (E)	$Kg \cdot J \cdot mol^{-1}$
material constant ($\tilde{\gamma}$)	$N \cdot m^{-2}$	Power law index (n)	$N \cdot m^{-2}$
Magnetic field (B_0)	$Kg \cdot s^{-2} \cdot A^{-1}$	cell swimming speed (Wc)	$m \cdot s^{-1}$
Density (ρ)	$Kg \cdot m^{-3}$	Temperature (T)	K
Angles (ω, Ω)	Radian	Concentration (C)	$Mol \cdot m^{-3}$
Thermal conductivity (k_f)	$W \cdot m^{-1} \cdot K^{-1}$	microorganisms concentration (N)	$Mol \cdot m^{-3}$
Thermophoresis diffusion (D)	$m^2 \cdot s^{-1}$	curvature parameter (γ)	m^{-1}
Brownian diffusion (\bar{D})	$m^2 \cdot s^{-1}$	An unsteadiness parameter (A)	$m \cdot s^{-1}$
Heat capacity (C_p)	$J \cdot Kg^{-1} \cdot K^{-1}$	Buoyancy force (Nr)	$Kg \cdot m^2$
Reaction rate (k_r)	$mol \cdot s^{-1}$	Electrical conductivity (σ)	$Sem \cdot m^{-1}$
Temperature difference (δ)	K	-	-

References

1. Nabwey Hossam, A.; Alshber, S.I.; Rashad, A.M.; Mahdy, A.E.N. Influence of bioconvection and chemical reaction on magneto—Carreau nanofluid flow through an inclined cylinder. *Mathematics* **2022**, *10*, 504. [[CrossRef](#)]
2. Ayub, A.; Sabir, Z.; Shah, S.Z.H.; Wahab, H.A.; Sadat, R.; Ali, M.R. Effects of homogeneous-heterogeneous and Lorentz forces on 3-D radiative magnetized cross nanofluid using two rotating disks. *Int. Commun. Heat Mass Transf.* **2022**, *130*, 105778. [[CrossRef](#)]
3. Shah, S.L.; Ayub, A.; Dehraj, S.; Wahab, H.A.; Sagayam, K.M.; Ali, M.R.; Sadat, R.; Sabir, Z. Magnetic dipole aspect of binary chemical reactive Cross nanofluid and heat transport over composite cylindrical panels. *Waves Random Complex Media* **2022**, 1–24. [[CrossRef](#)]
4. Ayub, A.; Sabir, Z.; Wahab, H.A.; Balubaid, M.; Mahmoud, S.R.; Ali, M.R.; Sadat, R. Analysis of the nanoscale heat transport and Lorentz force based on the time-dependent Cross nanofluid. *Eng. Comput.* **2022**, 1–20.

5. Imran, M.; Farooq, U.; Waqas, H.; Anqi, A.E.; Safaei, M.R. Numerical performance of thermal conductivity in Bioconvection flow of cross nanofluid containing swimming microorganisms over a cylinder with melting phenomenon. *Case Stud. Therm. Eng.* **2021**, *26*, 101181. [[CrossRef](#)]
6. Hosseinzadeh, K.; Roghani, S.; Mogharrebi, A.; Asadi, A.; Waqas, M.; Ganji, D. Investigation of cross-fluid flow containing motile gyrotactic microorganisms and nanoparticles over a three-dimensional cylinder. *Alex. Eng. J.* **2020**, *59*, 3297–3307. [[CrossRef](#)]
7. Ali, M.; Sultan, F.; Khan, W.A.; Shahzad, M.; Arif, H. Important features of expanding/contracting cylinder for Cross magneto-nanofluid flow. *Chaos Solitons Fractals* **2020**, *133*, 109656. [[CrossRef](#)]
8. Khan, N.S.; Humphries, U.W.; Kumam, W.; Kumam, P.; Muhammad, T. Bioconvection Casson nanoliquid film sprayed on a stretching cylinder in the portfolio of homogeneous—Heterogeneous chemical reactions. *ZAMM-J. Appl. Math. Mech./Z. Für Angew. Math. Mech.* **2022**, *102*, e202000222. [[CrossRef](#)]
9. Gopal, D.; Munjam, S.R.; Kishan, N. Analytical impact of Carreau nanofluid model under the influence of chemical reaction, Soret and Dufour over inclined stretching cylinder. *Int. Commun. Heat Mass Transf.* **2022**, *135*, 106148. [[CrossRef](#)]
10. Khan, M.; Yasir, M.; Alshomrani, A.S.; Sivasankaran, S.; Aladwani, Y.R.; Ahmed, A. Variable heat source in stagnation-point unsteady flow of magnetized Oldroyd-B fluid with cubic autocatalysis chemical reaction. *Ain Shams Eng. J.* **2022**, *13*, 101610. [[CrossRef](#)]
11. Lim, Y.J.; Shafie, S.; Isa, S.M.; Rawi, N.A.; Mohamad, A.Q. Impact of chemical reaction, thermal radiation and porosity on free convection Carreau fluid flow towards a stretching cylinder. *Alex. Eng. J.* **2022**, *61*, 4701–4717. [[CrossRef](#)]
12. Liu, C.; Khan, M.U.; Ramzan, M.; Chu, Y.M.; Kadry, S.; Malik, M.Y.; Chinram, R. Nonlinear radiative Maxwell nanofluid flow in a Darcy–Forchheimer permeable media over a stretching cylinder with chemical reaction and bioconvection. *Sci. Rep.* **2021**, *11*, 9391. [[CrossRef](#)] [[PubMed](#)]
13. Alarabi, T.H.; Rashad, A.M.; Mahdy, A. Homogeneous–heterogeneous chemical reactions of radiation hybrid nanofluid flow on a cylinder with joule heating: Nanoparticles shape impact. *Coatings* **2021**, *11*, 1490. [[CrossRef](#)]
14. Shahid, A.; Bhatti, M.M.; Ellahi, R.; Mekheimer, K.S. Numerical experiment to examine activation energy and bi-convection Carreau nanofluid flow on an upper paraboloid porous surface: Application in solar energy. *Sustain. Energy Technol. Assess.* **2022**, *52*, 102029. [[CrossRef](#)]
15. Mekheimer, K.S.; Shankar, B.M.; Ramadan, S.F.; Mallik, H.E.; Mohamed, M.S. On the stability of convection in a non-newtonian vertical fluid layer in the presence of gold nanoparticles: Drug agent for chemotherapy. *Mathematics* **2021**, *9*, 1302. [[CrossRef](#)]
16. Zaher, A.Z.; Ali, K.K.; Mekheimer, K.S. Electroosmosis forces EOF driven boundary layer flow for a non-Newtonian fluid with planktonic microorganism: Darcy Forchheimer model. *Int. J. Numer. Methods Heat Fluid Flow* **2021**, *31*, 2534–2559. [[CrossRef](#)]
17. Elogail, M.A.; Mekheimer, K.S. Modulated viscosity-dependent parameters for MHD blood flow in microvessels containing oxytactic microorganisms and nanoparticles. *Symmetry* **2020**, *12*, 2114. [[CrossRef](#)]
18. Mekheimer, K.S.; Ramadan, S.F. New insight into gyrotactic microorganisms for bio-thermal convection of Prandtl nanofluid over a stretching/shrinking permeable sheet. *SN Appl. Sci.* **2020**, *2*, 450. [[CrossRef](#)]
19. Aly, M.A.; El-Sapa, S. Effects of Soret and Dufour numbers on MHD thermosolutal convection of a nanofluid in a finned cavity including rotating circular cylinder and cross shapes. *Int. Commun. Heat Mass Transf.* **2022**, *130*, 105819. [[CrossRef](#)]
20. Zeeshan, A.; Mehmood, O.U.; Mabood, F.; Alzahrani, F. Numerical analysis of hydromagnetic transport of Casson nanofluid over permeable linearly stretched cylinder with Arrhenius activation energy. *Int. Commun. Heat Mass Transf.* **2022**, *130*, 105736. [[CrossRef](#)]
21. Ramzan, M.; Shaheen, N.; Chung, J.D.; Kadry, S.; Chu, Y.M.; Howari, F. Impact of Newtonian heating and Fourier and Fick’s laws on a magnetohydrodynamic dusty Casson nanofluid flow with variable heat source/sink over a stretching cylinder. *Sci. Rep.* **2021**, *11*, 2357. [[CrossRef](#)] [[PubMed](#)]
22. Poply, V.; Devi, R. A two—Component modeling for free stream velocity in magnetohydrodynamic nanofluid flow with radiation and chemical reaction over a stretching cylinder. *Heat Transf.* **2021**, *50*, 3603–3619.
23. Ibrahim, W.; Negera, M. Viscous dissipation effect on mixed convective heat transfer of MHD flow of Williamson nanofluid over a stretching cylinder in the presence of variable thermal conductivity and chemical reaction. *Heat Transf.* **2021**, *50*, 2427–2453. [[CrossRef](#)]
24. Gharami, P.P.; Arifuzzaman, S.M.; Khan, M.; Sarkar, T.; Ahmmed, S.F. MHD effect on unsteady flow of tangent hyperbolic nano-fluid past a moving cylinder with chemical reaction. *SN Appl. Sci.* **2020**, *2*, 1256. [[CrossRef](#)]
25. Xiong, P.Y.; Hamid, A.; Chu, Y.M.; Khan, M.I.; Gowda, R.J.; Kumar, R.N.; Prasannakumara, B.C.; Qayyum, S. Dynamics of multiple solutions of Darcy–Forchheimer saturated flow of Cross nanofluid by a vertical thin needle point. *Eur. Phys. J. Plus* **2021**, *136*, 345. [[CrossRef](#)]
26. Punith Gowda, R.J.; Naveen Kumar, R.; Jyothi, A.M.; Prasannakumara, B.C.; Sarris, I.E. Impact of binary chemical reaction and activation energy on heat and mass transfer of marangoni driven boundary layer flow of a non-Newtonian nanofluid. *Processes* **2021**, *9*, 702. [[CrossRef](#)]
27. Gowda, R.P.; Kumar, R.N.; Aldalbahi, A.; Issakhov, A.; Prasannakumara, B.C.; Rahimi-Gorji, M.; Rahaman, M. Thermophoretic particle deposition in time-dependent flow of hybrid nanofluid over rotating and vertically upward/downward moving disk. *Surf. Interfaces* **2021**, *22*, 100864. [[CrossRef](#)]

28. Varun Kumar, R.S.; Gunderi Dhananjaya, P.; Naveen Kumar, R.; Punith Gowda, R.J.; Prasannakumara, B.C. Modeling and theoretical investigation on Casson nanofluid flow over a curved stretching surface with the influence of magnetic field and chemical reaction. *Int. J. Comput. Methods Eng. Sci. Mech.* **2022**, *23*, 12–19. [[CrossRef](#)]
29. Sabir, Z.; Ayub, A.; Guirao, J.L.; Bhatti, S.; Shah, S.Z.H. The effects of activation energy and thermophoretic diffusion of nanoparticles on steady micropolar fluid along with Brownian motion. *Adv. Mater. Sci. Eng.* **2020**, *2020*, 2010568. [[CrossRef](#)]
30. Shah SZ, H.; Ayub, A.; Sabir, Z.; Adel, W.; Shah, N.A.; Yook, S.J. Insight into the dynamics of time-dependent cross nanofluid on a melting surface subject to cubic autocatalysis. *Case Stud. Therm. Eng.* **2021**, *27*, 101227. [[CrossRef](#)]
31. Kumar, R.N.; Gowda, R.P.; Alam, M.M.; Ahmad, I.; Mahrous, Y.M.; Gorji, M.R.; Prasannakumara, B.C. Inspection of convective heat transfer and KKL correlation for simulation of nanofluid flow over a curved stretching sheet. *Int. Commun. Heat Mass Transf.* **2021**, *126*, 105445. [[CrossRef](#)]
32. Darvesh, A.; Sajid, T.; Jamshed, W.; Ayub, A.; Shah, S.Z.; Eid, M.R.; Hussain, S.M.; Akram, M.; Hafeez, M.B.; Krawczuk, M. Rheology of Variable Viscosity-Based Mixed Convective Inclined Magnetized Cross Nanofluid with Varying Thermal Conductivity. *Appl. Sci.* **2022**, *12*, 9041. [[CrossRef](#)]
33. Varun Kumar, R.S.; Alhadhrami, A.; Punith Gowda, R.J.; Naveen Kumar, R.; Prasannakumara, B.C. Exploration of Arrhenius activation energy on hybrid nanofluid flow over a curved stretchable surface. *ZAMM-J. Appl. Math. Mech./Z. Für Angew. Math. Mech.* **2021**, *101*, e202100035. [[CrossRef](#)]
34. Ayub, A.; Wahab, H.A.; Shah, S.Z.; Shah, S.L.; Darvesh, A.; Haider, A.; Sabir, Z. Interpretation of infinite shear rate viscosity and a nonuniform heat sink/source on a 3D radiative cross nanofluid with buoyancy assisting/opposing flow. *Heat Transf.* **2021**, *50*, 4192–4232. [[CrossRef](#)]
35. Ayub, A.; Sabir, Z.; Altamirano, G.C.; Sadat, R.; Ali, M.R. Characteristics of melting heat transport of blood with time-dependent cross-nanofluid model using Keller–Box and BVP4C method. *Eng. Comput.* **2022**, *38*, 3705–3719. [[CrossRef](#)]
36. Jyothi, A.M.; Kumar, R.N.; Gowda, R.P.; Prasannakumara, B.C. Significance of Stefan blowing effect on flow and heat transfer of Casson nanofluid over a moving thin needle. *Commun. Theor. Phys.* **2021**, *73*, 095005. [[CrossRef](#)]
37. Sarada, K.; Gamaoun, F.; Abdulrahman, A.; Paramesh, S.O.; Kumar, R.; Prasanna, G.D.; Gowda, R.P. Impact of exponential form of internal heat generation on water-based ternary hybrid nanofluid flow by capitalizing non-Fourier heat flux model. *Case Stud. Therm. Eng.* **2022**, *38*, 102332.
38. Kumar, R.N.; Gamaoun, F.; Abdulrahman, A.; Chohan, J.S.; Gowda, R.P. Heat transfer analysis in three-dimensional unsteady magnetic fluid flow of water-based ternary hybrid nanofluid conveying three various shaped nanoparticles: A comparative study. *Int. J. Mod. Phys. B* **2022**, *36*, 2250170. [[CrossRef](#)]
39. Ayub, A.; Sajid, T.; Jamshed, W.; Zamora, W.R.; More, L.A.; Talledo, L.M.; Rodríguez Ortega de Peña, N.I.; Hussain, S.M.; Hafeez, M.B.; Krawczuk, M. Activation Energy and Inclination Magnetic Dipole Influences on Carreau Nanofluid Flowing via Cylindrical Channel with an Infinite Shearing Rate. *Appl. Sci.* **2022**, *12*, 8779. [[CrossRef](#)]
40. Ali, A.; Sarkar, S.; Das, S.; Jana, R.N. A report on entropy generation and Arrhenius kinetics in magneto-bioconvective flow of Cross nanofluid over a cylinder with wall slip. *Int. J. Ambient. Energy* **2022**, 1–16. [[CrossRef](#)]
41. Yin, J.; Zhang, X.; Rehman, M.I.U.; Hamid, A. Thermal radiation aspect of bioconvection flow of magnetized Sisko nanofluid along a stretching cylinder with swimming microorganisms. *Case Stud. Therm. Eng.* **2022**, *30*, 101771. [[CrossRef](#)]
42. Ramzan, M.; Shahmir, N.; Ghazwani, H.A. Stefan blowing impact on bioconvective Maxwell nanofluid flow over an exponentially stretching cylinder with variable thermal conductivity. *Waves Random Complex Media* **2022**, 1–16. [[CrossRef](#)]
43. Abdelmalek, Z.; Khan, S.U.; Waqas, H.; Riaz, A.; Khan, I.A.; Tlili, I. A mathematical model for bioconvection flow of Williamson nanofluid over a stretching cylinder featuring variable thermal conductivity, activation energy and second-order slip. *J. Therm. Anal. Calorim.* **2021**, *144*, 205–217. [[CrossRef](#)]
44. Benos, L.T.; Karvelas, E.G.; Sarris, I.E. A theoretical model for the magnetohydrodynamic natural convection of a CNT-water nanofluid incorporating a renovated Hamilton–Crosser model. *Int. J. Heat Mass Transf.* **2019**, *135*, 548–560. [[CrossRef](#)]
45. Sarris, I.E.; Kassinos, S.C.; Carati, D. Large-eddy simulations of the turbulent Hartmann flow close to the transitional regime. *Phys. Fluids* **2007**, *19*, 085109. [[CrossRef](#)]
46. Sarris, I.; Tsiakaras, P.; Song, S.; Vlachos, N. A three-dimensional CFD model of direct ethanol fuel cells: Anode flow bed analysis. *Solid State Ion.* **2006**, *177*, 2133–2138. [[CrossRef](#)]
47. Karvelas, E.; Liosis, C.; Benos, L.; Karakasidis, T.; Sarris, I. Micromixing efficiency of particles in heavy metal removal processes under various inlet conditions. *Water* **2019**, *11*, 1135. [[CrossRef](#)]
48. Animasaun, I.L.; Pop, I. Numerical exploration of a non-Newtonian Carreau fluid flow driven by catalytic surface reactions on an upper horizontal surface of a paraboloid of revolution, buoyancy and stretching at the free stream. *Alex. Eng. J.* **2017**, *56*, 647–658. [[CrossRef](#)]
49. Muhammad, T.; Alamri, S.Z.; Waqas, H.; Habib, D.; Ellahi, R. Bioconvection flow of magnetized Carreau nanofluid under the influence of slip over a wedge with motile microorganisms. *J. Therm. Anal. Calorim.* **2021**, *143*, 945–957. [[CrossRef](#)]
50. Shafique, Z.; Mustafa, M.; Mushtaq, A. Boundary layer flow of Maxwell fluid in rotating frame with binary chemical reaction and activation energy. *Results Phys.* **2016**, *6*, 627–633. [[CrossRef](#)]
51. Mahdy, A.; Hady, F.M.; Mohamed, R.A.; Abo-zaid, O.A. Activation energy effectiveness in dusty Carreau fluid flow along a stretched cylinder due to nonuniform thermal conductivity property and temperature—Dependent heat source/sink. *Heat Transf.* **2021**, *50*, 5760–5778. [[CrossRef](#)]

52. Mahdy, A. Natural convection boundary layer flow due to gyrotactic microorganisms about a vertical cone in porous media saturated by a nanofluid. *J. Braz. Soc. Mech. Sci. Eng.* **2016**, *38*, 67–76. [[CrossRef](#)]
53. Yusuf, T.A.; Mabood, F.; Prasannakumara, B.C.; Sarris, I.E. Magneto-bioconvection flow of Williamson nanofluid over an inclined plate with gyrotactic microorganisms and entropy generation. *Fluids* **2021**, *6*, 109. [[CrossRef](#)]
54. Jamshed, W.; Aziz, A. Entropy Analysis of TiO₂-Cu/EG Casson Hybrid Nanofluid via Cattaneo-Christov Heat Flux Model. *Appl. Nanosci.* **2018**, *8*, 1–14.
55. Jamshed, W.; Nisar, K.S. Computational single phase comparative study of Williamson nanofluid in parabolic trough solar collector via Keller box method. *Int. J. Energy Res.* **2021**, *45*, 10696–10718. [[CrossRef](#)]
56. Pasha, A.A.; Islam, N.; Jamshed, W.; Alam, M.I.; Jameel, A.G.A.; Juhany, K.A.; Alsulami, R. Statistical analysis of viscous hybridized nanofluid flowing via Galerkin finite element technique. *Int. Commun. Heat Mass Transf.* **2022**, *137*, 106244. [[CrossRef](#)]
57. Hussain, S.M.; Jamshed, W.; Pasha, A.A.; Adil, M.; Akram, M. Galerkin finite element solution for electromagnetic radiative impact on viscid Williamson two-phase nanofluid flow via extendable surface. *Int. Commun. Heat Mass Transf.* **2022**, *137*, 106243. [[CrossRef](#)]
58. Akram, M.; Jamshed, W.; Goud, B.S.; Pasha, A.A.; Sajid, T.; Rahman, M.M.; Arshad, M.; Weera, W. Irregular heat source impact on Carreau nanofluid flowing via exponential expanding cylinder: A thermal case study. *Case Stud. Therm. Eng.* **2022**, *36*, 102190. [[CrossRef](#)]
59. Khan, M.; Saleh Alshomrani, A. Characteristics of melting heat transfer during flow of Carreau fluid induced by a stretching cylinder. *Eur. Phys. J. E* **2017**, *40*, 8.
60. Rangi, R.R.; Ahmad, N. Boundary Layer Flow past a Stretching Cylinder and Heat Transfer with Variable Thermal Conductivity. *Appl. Math.* **2012**, *3*, 205–209. [[CrossRef](#)]